Charge carrier photogeneration, trapping, and space-charge field formation in PVK-based photorefractive materials

T. K. Däubler
Max-Planck-Institut für Polymerforschung, Ackermannweg 10, D-55128 Mainz, Germany

R. Bittner and K. Meerholz
Institut für Physikalische Chemie, Universität München, Butenandtstrasse 5-13, D-81377 München, Germany

V. Cimrová
Institute of Macromolecular Chemistry, Academy of Sciences of the Czech Republic, 16206 Prague 6, Czech Republic

D. Neher*
Institut für Physik, Universität Potsdam, Am Neuen Palais 10, D-14469 Potsdam, Germany
(Received 18 October 1999)

We studied the dark conductivity (j_{dark}), the photoconductivity (j_{photo}), and the charge carrier photogeneration efficiency η of poly(*N*-vinylcarbazole)–based photorefractive (PR) materials with different glass-transition temperatures (T_g) and chromophore content (ρ_{CHR}). Measurements were carried out at wavelengths similar to those used in degenerate four-wave mixing (DFWM) and two-beam coupling (2BC) experiments. Both thick (37 μm) and thin samples ($\approx$1 μm) were analyzed. Photoconductivity experiments at different temperatures show that both j_{dark} and j_{photo} are thermally activated. For j_{dark} the activation is not related to the glass-transition temperature of the blends, whereas photocurrents exhibit a universal behavior with respect to $T_r = T_g - T$. The charge carrier photogeneration efficiency η was measured by xerographic discharge experiments. η was found to be independent of both T_g and of ρ_{CHR}. The photoconductivity gain factor *G* defined as the number of charge carriers measured in photoconductivity in relation to the number of carriers initially photogenerated as determined by the xerographic experiments is used to compare the results of photoconductivity and xerographic discharge experiments. *G* is found to be much smaller than unity even for thin samples, which indicates that the mean free path of the photogenerated charge carriers is less than 1 μm at photoelectrical equilibrium. Using Schildkraut's model for the space-charge field formation in organic PR materials, trap densities T_i of approximately 10^{17} cm^{-3} could be derived from *G*. The field and temperature dependence of T_i is independent of ρ_{CHR} and might account for the universal T_r dependence of j_{photo}. The estimated trap densities are used to calculate the first-order Fourier component of the space-charge field in the PR materials illuminated with a sinusoidal intensity pattern. Modifying Schildkraut's model so that the tilt between the applied electric field and the index of refraction grating is taken into account yields saturation fields of approximately 100 V/μm in agreement with findings from PR experiments. The dramatic decrease of the space-charge field when the temperature exceeds the glass-transition temperature of the blend is fully explained by a decrease in trap density. The fact that the trap density depends on the temperature with respect to T_g and not on the absolute temperature suggests that the relevant traps are most likely of conformational nature.

INTRODUCTION

The photorefractive (PR) effect is defined as the spatial modulation of the index of refraction in an electro-optically active material due to the redistribution of charge carriers photogenerated under nonuniform illumination. For the buildup of the refractive index grating the following processes are necessary: (i) photogeneration of charge carriers, (ii) diffusion or drift of the mobile charge carriers, (iii) trapping of these charge carriers in the regions of low light intensity, and (iv) change of the index of refraction due to the buildup of an internal space-charge field. To relate a material's PR performance to these fundamental processes, (i) and (ii) can be studied by photoconductivity.[1–3] The electro-optical response (iv) has been investigated with ellipsometric techniques.[4]

In contrast to these intensively studied processes, charge trapping (iii) in PR polymers is less well understood. Even though trap densities have been extracted from two-beam coupling (2BC) experiments,[5–7] few attempts have been made to identify the trapping sites and to apply independent techniques to determine their density. Recently, absorption spectroscopy was used to determine the C_{60} radical anion concentration in C_{60}-sensitized PR polymers based on the photoconductor poly(*N*-vinylcarbazole) (PVK).[8] It was concluded that C_{60}^- acts as the primary hole trap, and trap densities determined by this simple spectroscopic method were in good agreement with those inferred from 2BC experiments. In analogy to the model for PVK/C_{60}, West *et al.* proposed a trapping mechanism for a PVK/2,4,7-trinitro-9-fluorenone system.[9] However, in this work no independent technique was employed to determine the trap density, and the proposed model is merely based on the comparison of blends containing different chromophores. In a polysiloxane/

TNF system photoconductivity experiments were used to independently determine the density of recombination centers.[10] The charged recombination sites were identified with occupied deep traps, and their density was in reasonable agreement with calculations from 2BC experiments. It should be noted that all trap densities (from either 2BC or independent experiments) were calculated using the standard model for photorefractivity that was developed for inorganic PR crystals.[11,12]

It is now well established that the index grating in organic PR materials can be further enhanced by the rotational mobility of the chromophores.[13] The effect of this ''orientational enhancement mechanism'' depends strongly on the plasticity, i.e., the glass-transition temperature (T_g) of the polymer.[14,15] Recently, we have studied the influence of T_g and chromophore content on the steady-state performance of PVK-based PR polymers by degenerate four-wave mixing (DFWM) experiments and ellipsometric techniques.[15] While the expected performance improvement with increasing chromophore content and decreasing T_g was confirmed for systems with T_g above room temperature, an optimum was observed for the highly doped systems with T_g close to room temperature (RT). It was demonstrated that this was the result of two counteracting effects: (i) the poling of the chromophore becomes more efficient with decreasing T_g, and (ii) the strength of the space-charge field E_{SC} decreases for T_g below room temperature. Based on the intensity dependence of the photocurrent, it was suggested that the decrease in E_{SC} is due to a reduced trap density for $T_g < \mathrm{RT}$.[15]

In this paper we investigate the photoresponse of the same PVK-based PR materials by photoconductivity (PC) and xerographic discharge (XD) experiments. By completing the characterization of the fundamental processes involved in the PR effect, a consistent picture of the photoconductivity, the charge carrier photogeneration efficiency, and the PR performance of PVK-based PR materials is provided. While the XD technique is known to be the most accurate method to determine the charge carrier photogeneration efficiency,[16,17] the transport and trapping properties of the materials can be further addressed by PC experiments. Due to these additional processes the photocurrent efficiency can deviate from the charge carrier photogeneration efficiency determined by XD experiments. The concept of photoconductivity gain can be used to relate the results of both techniques.[18–20] By employing Schildkraut's model for the space-charge field formation in organic PR materials,[21,22] a relation between the trap density and the photoconductivity gain factor is elaborated. Following this approach, measurements of the photocurrent and the charge carrier photogeneration efficiency of blends with different T_g and chromophore content are used to determine trap densities in the photoelectrical equilibrium. Finally, the same model is employed to predict the equilibrium photorefractive performance of these PVK-based PR materials.

EXPERIMENT

The investigated PR materials are based on the photoconductor poly(*N*-vinylcarbazole) (PVK), the electro-optic chromophore 2,5-dimethyl-4-(*p*-nitrophenylazo)anisole (DMNPAA), the plasticizer *N*-ethylcarbazole (ECZ), and the photosensitizer 2,4,7-trinitro-9-fluorenone (TNF) (Fig. 1).

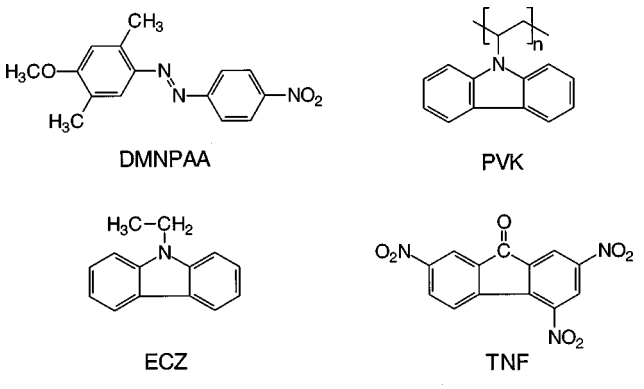

FIG. 1. Chemical structures of the different components in the PR blends used in this study: 2,5-dimethyl-4-(*p*-nitrophenylazo)-anisole (DMNPAA), poly(*N*-vinylcarbazole) (PVK), 2,4,7-trinitro-9-fluorenone (TNF), and *N*-ethylcarbazole (ECZ).

PVK secondary standard and ECZ were purchased from Aldrich. ECZ was purified by recrystallization, while PVK was used without further purification. DMNPAA was synthesized by azocoupling of a para-nitroaniline-diazonium salt with dimethylanisole and purified by column chromatography. T_g's of the blends were varied by changing the ratio of PVK/ECZ. The compositions and the corresponding T_g's of the investigated blends are listed in Table I. Glass-transition temperatures were derived from differential scanning calorimetry (DSC) measurements (with a heating rate of 20 K/min).

The devices for PC experiments were prepared by spin coating from toluene/cyclo-pentanone 4:1 mixtures on top of indium tin oxide–(ITO) coated glass substrates. The samples were kept in vacuum to remove residual solvent prior to evaporation of an Al top electrode. The photoconductivity of samples identical to those used for DFWM and 2BC experi-

TABLE I. Composition and glass-transition temperatures T_g of the investigated PVK-based PR materials.

System	ρ_{CHR}[a] (wt. %)	ρ_{PVK}[a] (wt. %)	ρ_{ECZ}[a] (wt. %)	T_g[b] (°C)
50a	50	50	0	35
50b	50	45	5	24.5*
50c	50	40	10	14
40a	40	60	0	72
40b	40	55	5	48.5*
40c	40	50	10	25
30z	30	70	0	120
30a	30	60	10	62
30b	30	55	15	37*
30c	30	50	20	12
20a	20	60	20	59.5*
20b	20	55	25	30
20c	20	50	30	14*

[a] ρ_{CHR}, ρ_{PVK}, ρ_{ECZ}: content of the chromophore DMNPAA, PVK and the plasticizer ECZ in the PR materials, respectively. For all systems ρ_{TNF} was 1 wt. %.

[b] Glass-transition temperatures T_g measured by DSC or interpolated between measured values (the latter are marked with an asterist).

ments was also measured. Those devices were prepared by melt pressing. The blends were sandwiched between two ITO-coated glass substrates at elevated temperature using 37-μm glass spacer beads to adjust the film thickness L. A strict preparation and measurement protocol was obeyed to obtain reproducible results.[23] Samples for xerographic discharge experiments were prepared by spin coating from toluene/cyclopentanone 4:1 solution on polished stainless-steel substrates. The thickness of the polymer layer was typically 1–2 μm.

Current-voltage (I-V) characteristics were recorded in dry nitrogen atmosphere in a temperature-stabilized setup.[24] For experiments under illumination a 689-nm diode laser with a photon flux of about 5×10^{17} photons/cm^2 s was used. Data were recorded pointwise and refer to currents established after the respective bias voltage was applied for 30 s. Dark currents, measured as a function of the electric field before and after experiments under illumination, were subtracted from currents measured under illumination to give the photocurrent ($j_{\text{photo}}=j_{\text{light}}-j_{\text{dark}}$). In the study presented here, the current was measured with a Keithley 617 electrometer and the voltage (-100 to 100 V) was supplied by the build-in voltage source.

XD experiments were performed with a self-constructed setup.[17] The sample was charged to the initial surface potential $U(t_0)=Q(t_0)/C$ by a corona process and then discharged upon irradiation. Here, $Q(t_0)$ is the surface charge density and C is the sample capacitance per unit area. $U(t)$ was recorded with a sampling frequency of 40 Hz. The photoinduced discharge quantum efficiency η' is calculated from

$$\eta' = -\frac{1}{e\Phi}\left(\frac{dQ}{dt}\right)_{t_0} = -\frac{1}{e\Phi}C\left(\frac{dU}{dt}\right)_{t_0}, \qquad (1)$$

where Φ is the absorbed photon flux density, e is the electron charge, $(dQ/dt)_{t_0}$ represents the rate of change of the surface charge density, and $(dU/dt)_{t_0}$ is the initial photoinduced discharge rate. Under emission-limited conditions (no recombination, no space charge effects), η' is independent of both sample thickness and light intensity and equals the charge carrier photogeneration efficiency η. To ensure emission-limited conditions, the incident photon flux was kept as low as possible (10^{13}–10^{14} photons/cm^2 s). A halogen lamp with various interference filters was used for illumination, except at 355 nm, for which a UV-CAMAG lamp was used. The measurements were performed with illumination upon the positively charged surface. All experiments were carried out at ambient conditions.

For each measurement presented here, the material compositions were carefully chosen to guarantee a good reproducibility of the experiments. One particular problem is that thin spin-coated films of blends with high chromophore concentration and low T_g are not very stable, since the chromophore tends to diffuse to the surface and subsequently crystallize at the film/air interface. The T_g dependence of the charge carrier photogeneration efficiency was measured on blends 20a ($T_g=59.5\,^\circ$C), 20b ($T_g=30\,^\circ$C), and 20c ($T_g=14\,^\circ$C) with a low chromophore concentration, while the effect of ρ_{CHR} on η was studied using the high-T_g blends 20a ($T_g=59.5\,^\circ$C), 30a ($T_g=62\,^\circ$C), and 40a ($T_g=72\,^\circ$C). Temperature-dependent studies of the photocurrent were conducted for thick devices of blends 20c ($T_g=14\,^\circ$C), 30c ($T_g=12\,^\circ$C), and 40b ($T_g=48.5\,^\circ$C). Since the maximum output voltage of the used electrometer is 100 V, the electric field strength in these experiments was rather low. Photocurrents at higher fields were recorded on spin-coated samples of the high-T_g blends 30a, 30z ($T_g=120\,^\circ$C), and 40a. We are aware of the fact that these experimental limitations might affect the universality of the conclusions drawn below. There is, however, significant evidence that the photocurrent data can be parameterized in T_r, independent of the particular sample composition. Note that the carbazole concentration $\rho_{\text{carb}}=\rho_{\text{PVK}}+\rho_{\text{ECZ}}$ varies between 50 and 80 wt.% for the blends studied here, i.e., only by a factor of less than 2.

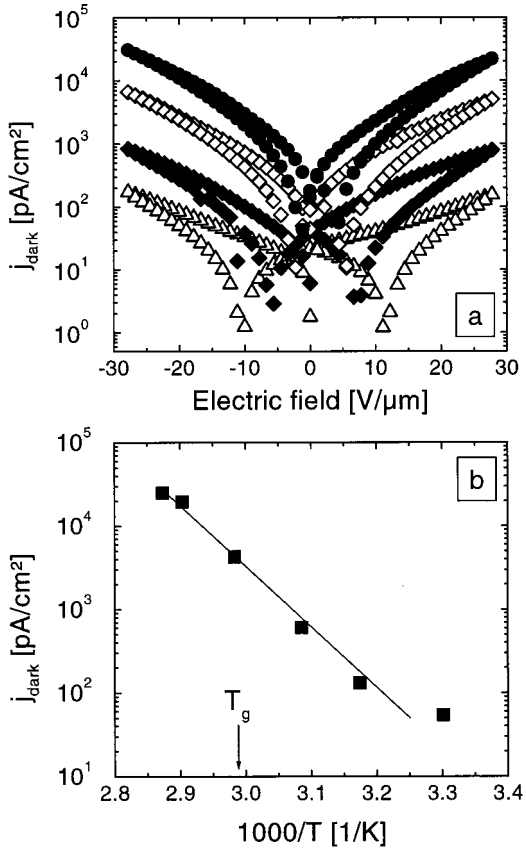

FIG. 2. (a) Dark I-V characteristics of a 0.9-μm-thick layer of blend 30a ($T_g=62\,^\circ$C) between an ITO bottom and an Al top electrode. j_{dark} was measured at 43 °C (△), 53 °C (◆), 65 °C (◇), and 75 °C (●). The measurements were performed in dry nitrogen atmosphere ($p=1$ bar), starting with negative polarity (ITO$^-$) from zero bias. (b) An Arrhenius plot of j_{dark} at a field of +25 V/μm. The solid line corresponds to an activation energy of 1.5 eV.

RESULTS

Figure 2 shows the field dependence of the dark current of a 0.9-μm-thick layer of blend 30a between an Au bottom and an Al top electrode. Even though the work functions of the bottom and top contacts are different, there was no signature of asymmetry or even rectification. The Arrhenius plot of the dark current at 25 V/μm gives a rather high activation en-

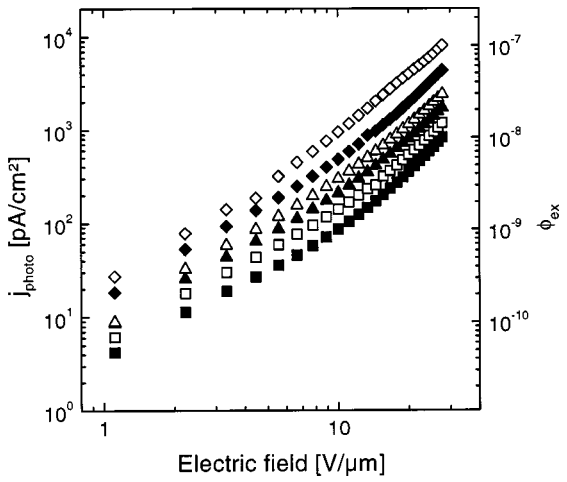

FIG. 3. *I-V* characteristics of the photocurrent of a 0.9-μm-thick sample of blend 30a ($T_g = 62\,^\circ$C). Currents were measured at 10 °C (■), 30 °C (□), 43 °C (▲), 53 °C (△), 65 °C (◆), and 75 °C (◇). The sample was illuminated through the ITO electrode with $\lambda = 689$ nm and a constant photon flux of 5×10^{17} photons/cm^2 s. Experiments were performed in dry N_2 with the ITO bottom electrode biased as the anode.

ergy of 1.5 eV. Note that there is no change in the thermal activation of the dark current as the temperature is increased above T_g.

The photocurrent j_{photo} of a 0.9-μm-thick sample of blend 30a as a function of the field at different temperatures is shown in Fig. 3. The field dependence of the photocurrent is linear at low fields and quadratic at high fields. For all samples the currents under illumination were much larger than dark currents for measurements at room temperature. j_{photo} and j_{dark} became comparable only at high temperatures due to the large activation energy of j_{dark}, but they still could be clearly distinguished. Also shown is the external photocurrent efficiency ϕ_{ex}, defined as the number of measured charge carriers per incident photon:

$$\phi_{\text{ex}} = \frac{hc}{e\lambda}\frac{j_{\text{photo}}}{I}, \tag{2}$$

where I is the light intensity and λ the wavelength of light.

The temperature dependence of the photocurrents is compared for different samples in Fig. 4. For all three materials shown, there is a pronounced increase in j_{photo} above T_g. When plotted as a function of the reduced temperature $T_r = T_g - T$, the data show a universal behavior for all three samples. Thus, j_{photo} is mainly a function of the temperature with respect to T_g and does not strongly depend on the chromophore or the plasticizer content.

The field dependence of the charge carrier photogeneration efficiencies η for PR blends with different T_g's and chromophore content is compiled in Fig. 5. In the analysis of the xerographic data only the absorption of PVK/TNF was taken into account. Absorption spectra of a PR blend and of the same material without the sensitizer are shown in Fig. 6. The absorption is governed by the chromophore in the short-wavelength range but exhibits clear signatures of the PVK/TNF charge-transfer (CT) complex at longer wavelengths.

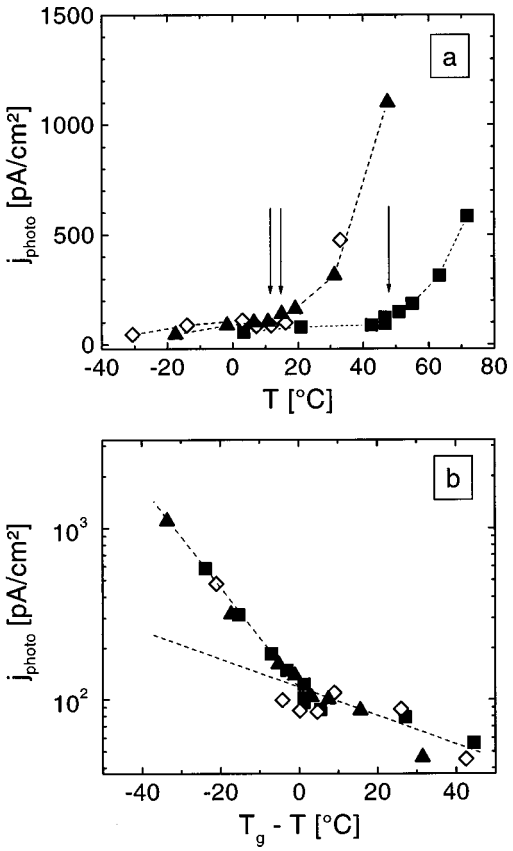

FIG. 4. (a) Photocurrent as a function of temperature at a field of 1 V/μm for blend 20c (▲; $T_g = 14\,^\circ$C), blend 30c (◇; $T_g = 12\,^\circ$C), and blend 40b (■; $T_g = 48.5\,^\circ$C). Measurements were performed on 37-μm-thick films between ITO electrodes. Illumination was at $\lambda = 689$ nm with a constant photon flux of 5×10^{17} photons/cm^2 s. Arrows indicate the glass-transition temperatures of the materials. (b) Same data plotted as a function of the reduced temperature $T_r = T_g - T$.

Absorption coefficients of the CT complex only are shown in the inset. These data were obtained by subtracting spectra recorded on materials without TNF from the spectra of the PR blend with TNF. In Fig. 5 no dependence of η on the chromophore content and the glass-transition temperature can be observed. The field dependence of η is well described by Onsager's theory as outlined below. Note that the absorption of the chromophore is still low at 580 nm and does not significantly attenuate the incident light in the ~2-μm-thick samples.

The field dependence of η of a PVK/TNF film (2 wt. % TNF) was analyzed (Fig. 7) to compare the results obtained on the PR blends, where only the absorption of the CT complex was used in the XD-data analysis, to a system that only contains PVK and TNF. Measurements were performed with illumination in the absorption range of PVK and with wavelengths, for which only the PVK/TNF CT complex absorbs. Note that the experimental error in the latter case is much higher due to the low absorption coefficient. Furthermore, the error decreases with increasing electric field. Taking this into account, only a weak dependence of the charge carrier photogeneration efficiency on the excitation wavelength is observed. The field dependence of η is again well described by Onsager's theory.

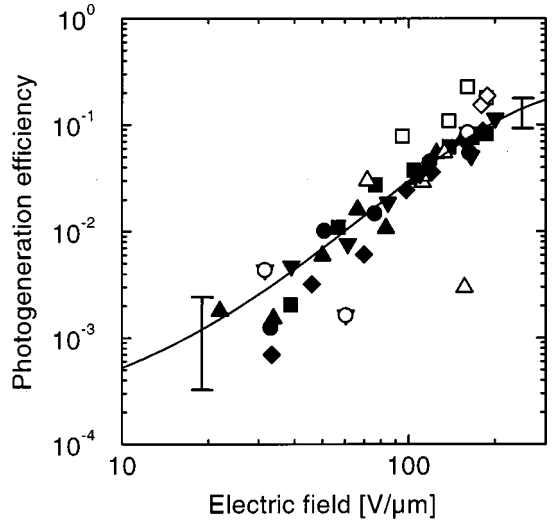

FIG. 5. Field dependence of the charge carrier photogeneration efficiency η for PR blends with different T_g and chromophore content ρ_{CHR}: blend 20a ($T_g=59.5\,°C$; $d=1.1\,\mu m$; ▲, △), blend 20b ($T_g=30\,°C$; $d=0.9\,\mu m$; ◆, ◇), blend 20c ($T_g=14\,°C$; $d=0.95\,\mu m$; ■; □), blend 30a ($T_g=62\,°C$, $d=0.95\,\mu m$; ▼, ▽), and blend 40a ($T_g=72\,°C$; $d=1.0\,\mu m$; ●, ○). Data were obtained by xerographic discharge with illumination at 580 nm (filled symbols) and 671 nm (open symbols). η was calculated using only the absorption of the carbazole:TNF charge transfer complex. The experimental error is indicated for low and the high electric fields. The solid line is a fit using Onsager's theory with a δ distribution of the initial CT radii. The fitting parameters are listed in Table II.

DISCUSSION

Dark-current behavior

Dark-current–voltage characteristics were measured to investigate the effect of the glass-transition temperature and the composition of the PR blends on j_{dark}. In these experiments no correlation between j_{dark} and T_g was found. The Arrhenius plot of the dark current gives a high activation energy (E_A) of 1.5 eV, which does not change as the temperature is raised above T_g [Fig. 2(b)]. Similar results were obtained for PR materials with different chromophore content and different T_g's. Three different basic processes may govern j_{dark}: (i) thermal bulk generation, (ii) injection from the electrodes and injection-limited current, (iii) injection from the electrodes and transport-limited currents. From our data we can neither prove nor safely exclude any of these three processes. Thermal bulk generation is supported by the large activation energy, but the pronounced field dependence of the dark current is difficult to explain under this assumption. Injection-limited currents are unlikely since the I-V characteristics are symmetric even though an asymmetric device geometry was used. The difference between the work functions of the ITO ($\phi\approx 4.6-4.9\,eV$) and Al ($\phi\approx 4.1-4.3\,eV$) electrode[25] should give rise to asymmetric or even rectified I-V characteristics at low fields, neither of which are observed experimentally [Fig. 2(a)]. Process (iii) is supported by the finding that the average dark current (average of j_{dark} for increasing and decreasing field) is proportional to E^2 for $E>10\ V/\mu m$, which might indicate space-charge limited current (SCLC) behavior, i.e., transport-limited currents. However, the analysis of the data for different PR blends using Child's law for SCLC,[26–28]

$$j_{SCLC}=\tfrac{9}{8}\,\epsilon_0\epsilon\mu_{eff}\frac{U^2}{L^3}, \tag{3}$$

results in very small mobilities μ_{eff} of $10^{-13}-10^{-10}\,cm^2/V\,s$. These values are far below the typical hole mobilities in PVK systems ($10^{-7}-10^{-5}\,cm^2/V\,s$).[29,30]

One possible explanation is that the dark current is governed by the transport of injected electrons via deep traps,

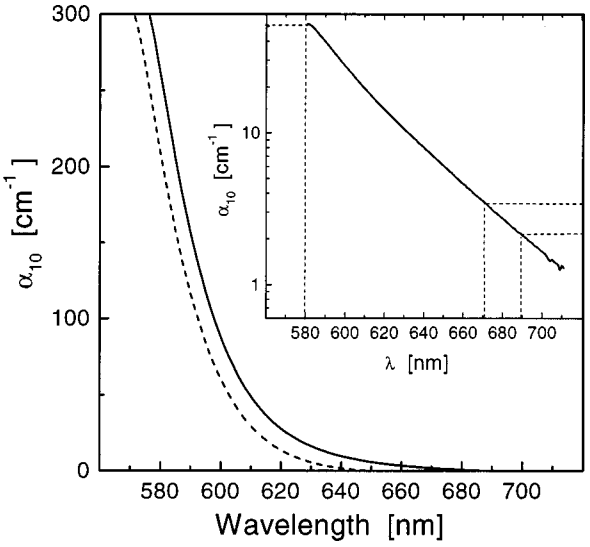

FIG. 6. Absorption spectra of a PR blend with 50 wt. % DMNPAA, 42 wt. % PVK, 7 wt. % ECZ, and 1 wt. % TNF (solid line) and of the same material without TNF (dashed line). The absorption coefficients of the PVK/TNF charge-transfer complex in the blends is shown in the inset. The data were calculated by subtracting the spectra without TNF from the spectra of the PR blend with TNF.

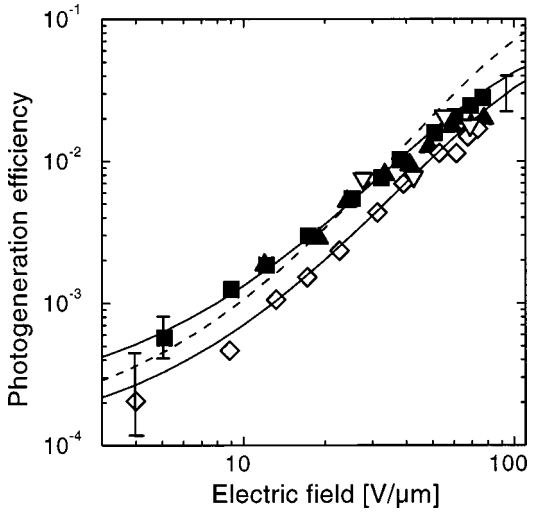

FIG. 7. Field dependence of the charge carrier photogeneration efficiency η determined by XD experiments for a 2.5-μm-thick film of PVK/TNF (2 wt. %). The sample was illuminated at 355 nm (■), 385 nm (▲), 510 nm (◇), and 671 nm (▽). The experimental error is indicated for low and the high electric fields. Solid lines are fits to Onsager's theory with a δ-distribution of the initial CT radii. The fit parameters are listed in Table II. Also shown is a fit (dashed line) using the data by Melz (Ref. 32) ($\epsilon=3.0$, $r_0=3.5\,nm$, $\eta_0=0.23$).

possibly the sensitizer or the chromophore. The absence of a T_g effect in the temperature dependence of j_{dark} and the pronounced hysteresis effects for low temperatures and fields suggest the presence of deep traps. A consistent description of the dark-current behavior requires further experiments with different contacts, which will be the subject of forthcoming work.

Photocurrent characteristics

Experiments at different temperatures clearly show that photocurrents are also thermally activated. In contrast to j_{dark}, the increase of j_{photo} with temperature is significantly accelerated above the glass-transition temperature. Independent of the chromophore concentration, j_{photo} is mainly a function of the measurement temperature relative to T_g [Fig. 4(b)] but not of the absolute temperature.

Xerographic discharge experiments

The analysis of the xerographic data taking into account only the photons absorbed by the carbazole/TNF CT complex yields photogeneration efficiencies that are almost independent of the chromophore content and the glass-transition temperature (Fig. 5). Since the fraction of photons absorbed by the chromophore varies significantly for the studied samples (more than a factor of 2 going from 20 to 50 wt. % DMNPAA), the close similarity of the photogeneration efficiencies indicates that the chromophore does not significantly contribute to charge carrier photogeneration. XD experiments on blends containing no TNF indeed show much smaller generation efficiencies. For example, in samples with 20 wt. % chromophore content and without TNF, $\eta = 1.1 \times 10^{-5}$ and 6.2×10^{-4} at $E = 10$ and 53 V/μm, respectively, for $\lambda = 480$ nm. Note that the total absorption coefficient is an order of magnitude higher at this wavelength compared to $\lambda = 580$ nm and that we have used the chromophore absorption coefficient in the XD-data analysis in this case. The absence of a ρ_{CHR} dependence of η confirms the conclusions drawn from photoconductivity experiments. The finding that η is, furthermore, independent of T_g allows us to exclude contributions of a T_g-dependent photogeneration efficiency to the universal T_r dependence of j_{photo}. Thus, the changes in j_{photo} are most likely related to changes in the transport and recombination properties with T_g.

Charge carrier photogeneration efficiencies in the PR blends are approximately 3% at a field of 100 V/μm (Fig. 6). As η is almost proportional to E^2, the efficiency decreases rapidly with decreasing field to only 0.7% at 50 V/μm. Furthermore, the generation efficiency is the same for illumination with 580 and 671 nm. One might presume that large errors can be caused by irradiating at a wavelength with low absorption. In this case light penetrates through the whole sample and the requirement of emission-limited discharge may no longer be met. Thus, the analysis of the xerographic data might yield incorrect values of the absolute photogeneration efficiency.

To investigate the effect of penetration depth on the determination of the charge carrier photogeneration efficiency arising from the absorption of the PVK/TNF complex, we carried out XD experiments on a 2.5-μm-thick layer of PVK doped with 2% TNF. Measurements were performed for illumination in the wavelength range of strong absorption, within the PVK absorption range, as well as below the polymer absorption band. Previous investigations by Andre, Lever, and Moisan[31] showed that η measured at a field of 50 V/μm is almost independent of wavelength for illumination between 400 and 650 nm and decreases for excitation wavelengths longer than 700 nm. In agreement with this, η depends only slightly on the excitation wavelength in our experiments (Fig. 7). The fit to Onsager's model with a single CT radius r_0 indicates that this difference is mainly due to a slightly smaller value of r_0 at longer wavelength while the primary quantum yield η_0 is constant (Table II). The obtained fit parameters are in good agreement with published data.[32]

TABLE II. Fit parameters for the electric field dependence of the charge carrier photogeneration efficiency in PVK/TNF and photorefractive blends at different illumination wavelengths. A δ function was used for the distribution of the initial CT radii (r_0) in Onsager's model. ϵ is the dielectric constant and η_0 the primary quantum yield.

System	λ_{exc} (nm)	ϵ	r_0 (nm)	η_0
PVK/TNF (2 wt. %)	355, 385	3.5	2.6	0.1
	510	3.5	2.35	0.1
PR blend (1 wt. % TNF)	580	5.5	1.3	0.35

Note that absolute quantum efficiencies are similar for PR blends and the PVK/TNF system. However, the Onsager fit to the photogeneration efficiency in the PR materials yields a smaller CT radius and a higher η_0 than those in PVK/TNF. In the former case, a higher dielectric constant $\epsilon = 5.5$ has been used, which represents a typical value measured for blends containing 20–30 wt. % DMNPAA.[15] Fitting the same data with a lower value for ϵ would yield a larger r_0 and a lower η_0. Note that the separation of charge carriers occurs in a rather local environment within nanoseconds. Thus, the correct choice of ϵ in the Onsager fit might differ from the macroscopically measured value.

Determination of the trap density

For a given electric field, the photogeneration efficiency η as determined by XD experiments is several orders of magnitude higher than the external photocurrent efficiency ϕ_{ex} calculated from j_{photo} (Figs. 3 and 5). The objective of the following discussion is to provide a consistent picture of the photoconductivity, the charge carrier photogeneration, and the PR performance of the same materials as published earlier.[15] This will be achieved by relating ϕ_{ex} to η and to the trap density in the material.

Commonly, Kukhtarev's model for photorefractivity in inorganic crystals is used to describe the PR effect in polymeric systems.[11,12] An alternative model developed by Schildkraut and co-workers[21,22] includes several features typical for organic PR compounds. Its basic concept is depicted in Fig. 8. Mobile holes are generated solely by photoexcitation of neutral sensitizer molecules [initial density S_i; generation rate $g(E)$]. Thermal generation and charge carrier injection are neglected. Upon excitation free holes and negatively charged sensitizer molecules S^- are gener-

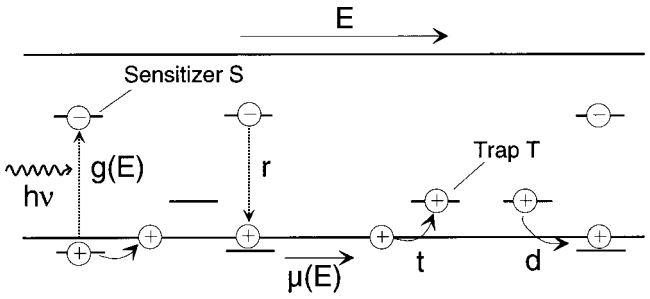

FIG. 8. Schematic representation of Schildkraut's model for the photorefractive effect in organic materials. Initially, all sensitizer molecules (initial density S_i) are neutral and all hole traps (initial density T_i) are empty and neutral. Under illumination, holes are photogenerated with a field-dependent rate $g(E)$. For every photogenerated hole, a negatively charged sensitizer molecule is generated. The motion of the holes is described by a field-dependent mobility $\mu(E)$. r is the recombination rate of photogenerated holes with negatively charged sensitizer molecules. Holes can be captured by traps with a trapping rate t. The detrapping rate back to the hole transport band is d.

ated. The latter can act as recombination centers for the free holes (recombination rate r). The mobile holes might, furthermore, be captured by traps (initial density T_i; trapping rate t). Finally, trapped carriers might be detrapped by thermal activation (detrapping rate d). While the general set of coupled equations can only be solved numerically,[21] Schildkraut and Cui gave zero- and first-order analytical expressions for either the case of deep traps (no detrapping) or no traps ($T=0$).[22] In the following, only the deep trap limit will be discussed. Since all equations and results by Schildkraut and co-workers are in dimensionless form, the most important expressions are translated into SI units in the following. (A detailed treatment of Schildkraut's model in SI units is given in Ref. 33.)

The photogeneration rate $g(E)$ is expressed by

$$g(E)=\eta(E)\frac{\alpha I}{\hbar\omega}, \tag{4}$$

where η is the charge carrier photogeneration efficiency, α is the absorption coefficient due to the sensitizer molecules, I is the light intensity, and $\hbar\omega$ the photon energy. It is assumed that η and the hole mobility μ are field dependent, and

$$\mu=\mu^i\exp[C(\sqrt{E}-E_A/\beta)] \tag{5a}$$

is obtained from the disorder transport formalism discussed by Pautmeier, Richert, and Bässler.[34] μ^i is a constant and E_A is the activation energy at zero field. β and C are experimentally determined parameters. For the fields typically applied to organic PR materials, a power law

$$\eta(E)=\eta^i E^p \tag{5b}$$

serves as a good approximation to the Onsager field dependence as shown by Braun[35] and observed here for electric field strengths between 10 and 100 V/μm. η^i is a constant and p is an experimentally determined parameter.

The sample is illuminated by a sinusoidal fringe pattern with the light intensity $I(x)$ given by

$$I(x)=I_0[1+m\cos(Kx)], \tag{6}$$

where m is the contrast factor of the interference pattern, $K=2\pi/\Lambda$ is the grating vector in the x direction, and Λ is the grating spacing. The density of free holes is expanded in a Fourier series:

$$\rho=\rho_0+\rho_1\exp(iKx), \tag{7}$$

where we neglect time-dependent terms that characterize the grating formation, i.e., we only consider steady-state conditions. Expressions identical to Eq. (7) are written for all x-dependent variables.

In the limit of photostatic equilibrium all relevant traps are filled, independent of the position relative to the illumination grating (at this point we abstain from any assignment of the nature of these traps). As a consequence a fraction of the sensitizer molecules S^- equal to the trap density will remain ionized and act as recombination centers for holes. It is further assumed that the trap density is higher than the density of free holes such that

$$\rho_0 \ll T_i. \tag{8}$$

With the above assumptions the zero-order Fourier component of the hole density is given by

$$\rho_0=\rho^*\frac{S_i-T_i}{\rho^*+S_i-T_i}, \tag{9a}$$

$$\rho^*=\frac{\alpha\eta_0 I_0}{\hbar\omega}\frac{1}{\gamma T_i}. \tag{9b}$$

Here, ρ^* is the zero-order hole density for uniform illumination with a sufficiently small light intensity. η_0 is the photogeneration efficiency at a given external field E_0,

$$\eta_0=\eta^i E_0^p, \tag{10}$$

and γ is the coefficient for the recombination of holes with ionized sensitizer molecules S^- defined by

$$\frac{\partial\rho}{\partial t}=-\gamma S^-\rho=-\frac{\rho}{\tau_r}. \tag{11}$$

τ_r is the average lifetime of the holes. In organic solids the recombination of a free hole with an ionized sensitizer is described by Langevin recombination with the recombination coefficient γ given by[36]

$$\gamma=\frac{e\mu}{\epsilon_0\epsilon}. \tag{12}$$

For low illumination intensities the density of photogenerated holes is much smaller than the total density of sensitizer molecules S_i. If in addition $T_i \ll S_i$, the zero-order Fourier component of the hole density ρ_0 is equal to ρ^*.

In this case the photocurrent is given by

$$j_{\text{photo}}=e\rho^*\mu_0 E_0 \tag{13a}$$

$$=eGg(E_0)L, \tag{13b}$$

where L is the sample thickness and $g(E_0)$ is the generation rate at the external field E_0. In Eq. (13b) the photoconduc-

tivity gain factor G is used to express that the number of carriers flowing through the external circuit in steady-state photoconductivity experiments which can be larger or smaller than the number of primarily photogenerated charge carriers.[18,19] In any case, G is related to the internal photocurrent efficiency ϕ_{in}, defined as the number of charge carriers per absorbed photon, calculated from j_{photo},

$$\phi_{in} = G\,\eta, \tag{14}$$

which in the case of weak absorption is related to the external photocurrent efficiency ϕ_{ex}, defined by Eq. (2),

$$\phi_{in} = \frac{\phi_{ex}}{\ln 10\,\alpha_{10} L}. \tag{15}$$

Here, L is the thickness of the sample and α_{10} the absorption coefficient taken to log base 10. Using Eqs. (13) and (9b) and Eq. (12) for the Langevin recombination coefficient, the photoconductivity gain factor G can be related to the initial trap density T_i in Schildkraut's model:

$$G = \frac{\epsilon\epsilon_0 E_0}{eLT_i}. \tag{16}$$

By setting $S^- = T_i$ and using Eqs. (11) and (12), this expression translates into the well-known relation for G,[18,19]

$$G = \frac{\tau_r}{\tau_t}, \tag{17a}$$

with the carrier transit time τ_t given by

$$\tau_t = \frac{L}{\mu E}. \tag{17b}$$

With Eqs. (14), (15), and (16), the relation between ϕ_{ex} and η_0 becomes

$$\phi_{ex} = \ln 10\,\alpha_{10}\frac{\epsilon_0\epsilon E}{eT_i}\,\eta_0. \tag{18}$$

Note that a similar equation was derived by Bäuml *et al.*[10] for the density of recombination centers, which were identified with deep traps. The derivation in this work was based on an estimate of the lifetime of a photogenerated charge carrier before being trapped in a recombination center.

In order to determine T_i we plot the external and internal photocurrent efficiency for different samples as a function of the electric field. This is shown in Fig. 9 together with the field dependence of the charge carrier photogeneration efficiency η as derived from XD experiments. Since materials with different T_g's were used, all PC data were normalized to photocurrents at $T_r = 0$ using the data in Fig. 4. Also included are efficiencies as determined from earlier PC experiments at high fields (comparable to those in applied in XD experiments) on a 37-μm-thick samples (containing 50 wt. % chromophore) using an external high voltage (HV) voltage source.[15] For each data set, T_i (and thus G) was adjusted such that ϕ_{in}/G [Eq. (14)] is in good agreement with the predictions for η from the Onsager fits of the xerographic data. The resulting values of T_i and G are summarized in Table III. Note that for each sample, all data are rescaled using only one field-independent value for T_i. The field dependence of $\eta(E)$ as determined by the adjusted photocurrent data is in good agreement with the η-E curves predicted by Onsager's theory. However, the comparison of the low-field data ($E \approx 1$ V/μm) needs to be regarded carefully, since only the high-field XD data were considered in the Onsager fits. Charge carrier photogeneration efficiencies are comparable for the compounds with 30 and 40 wt. % DMNPAA over the entire investigated field range.

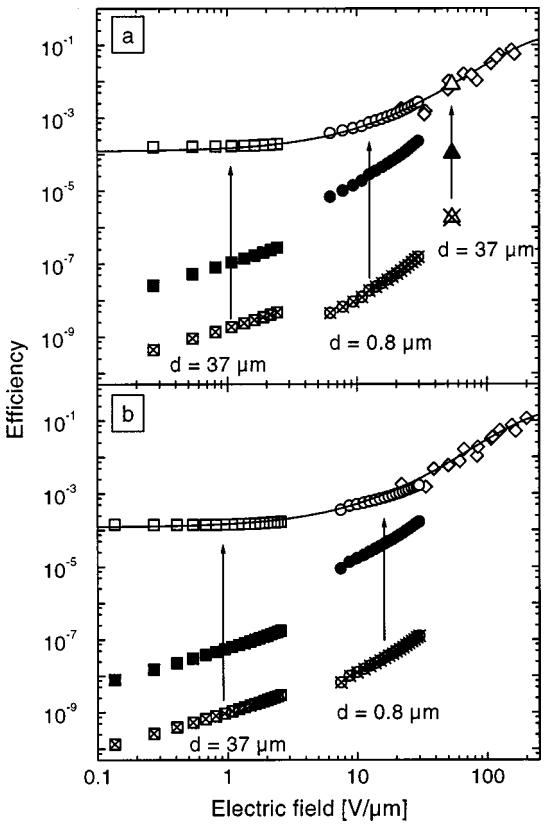

FIG. 9. (a) A comparison of the field dependence of the photogeneration efficiency η determined by XD experiments on a 1.0-μm-thick layer of blend 40a ($\diamond$) with calculated η (open symbols), the internal photocurrent efficiency ϕ_{in} (filled symbols), and the external photocurrent efficiency ϕ_{ex} (crossed symbols). The other symbols correspond to data obtained from PC measurements on blend 40b (37 μm; squares), blend 40a (0.8 μm; circles), and blend 50c (37 μm, triangles; taken from Ref. 15). The values of ϕ_{ex}, ϕ_{in}, and η were calculated according to Eqs. (2), (14), and (15). For each data set, the photoconductivity gain factor G was optimized using Eq. (16) to give a continuous dependence of η on the electric field. (b) The same comparison as (a) except that η is measured on blend 30a (0.95 μm; $\diamond$). The other symbols in (b) correspond to data calculated from PC measurements on blend 30c (37 μm; squares) and blend 30z (0.8 μm; circles) of η (open symbols), ϕ_{in} (filled symbols), and ϕ_{ex} (crossed symbols). The solid lines in (a) and (b) are fits using Onsager's theory with a δ distribution of CT radii. The fit parameters are the same as used for the master curve in Fig. 5 (Table II). The values of T_i and thus of G used to adjust the PC data to the field dependence of η are summarized in Table III.

For all samples G is much smaller than unity, even for a layer thickness of only 0.8 μm. This implies that only a small fraction of photogenerated charge carriers can diffuse over a distance of 1 μm. This seems to be in contrast to results from time-of-flight (TOF) and transient holographic diffraction experiments, which indicated free path lengths of

TABLE III. Parameters for the calculation of the photoconductivity gain in Fig. 9 according to Eq. (16) at an excitation wavelength $\lambda = 689$ nm.

System	L (μm)	ϵ	T_i (10^{17} cm^{-3})	G/E_0 (10^{-4} μm/V)
30c	37	5.3	0.20	3.96
30z	0.8	5.3	1.10	33.3
40b	37	5.9	0.15	5.88
40a	0.8	5.9	1.60	25.5
50a	37	6.5	0.44	2.21
50c	37	6.5	0.46	2.11

several micrometers.[30] However, those transient experiments were performed on ''fresh'' samples which were not in photostatic equilibrium. The low drift length in the steady-state PC experiments presented here were measured on samples that had previously been biased and exposed to light, resulting in a significant concentration of ionized sensitizer molecules acting as recombination centers. This behavior is exactly predicted by Schildkraut's model, where charged recombination centers are not initially present in the material, but must be generated by the photoexcitation of the sensitizer. Optical activation of deep trapping sites that may act as recombination centers was also observed by others.[8,37,38]

The adjustment of the photocurrent data yields values of $(0.15-0.5)\times 10^{17}$ cm^{-3} for T_i for samples with 37 μm thickness. However, for the thin spin-coated films $T_i > 10^{17}$ cm^{-3}. These values are in good agreement with trap densities determined in C_{60}-sensitized PR polymers by Grunnet-Jepsen *et al.*[8] and in TNF-containing guest-host polymers by Bäuml *et al.*[10] Even though the difference in T_i between the two types of samples (1 and 37 μm thickness) is not very large, it is consistent for all sets of samples studied here (Table III). It can be assumed that either a higher trap density at the interface to the electrodes or effects due to the injection of electrons from the Al top electrodes of the thin samples cause an overall increase in T_i. In the following discussion, a trap density $T_i \approx 5\times 10^{16}$ cm^{-3} at $T_r = 0$, as determined for the thick samples with 50-wt. % chromophore content and high fields will be used.

Estimates for the space-charge field

The estimated trap density can be used to predict the first-order Fourier component of the electric space-charge field E_1 caused by illumination with a perfect sinusoidal fringe pattern. In the limits outlined above, Schildkraut's model yields the following relation:

$$E_{SC} = E_1 = -mAE_q \frac{E_0 - iE_D}{\left[E_D + (1+pA)E_q + \left(1+\frac{E_m}{E_0}\right)E_j\right] + i\left[E_0 + \frac{E_D E_q}{E_0}\left(\frac{E_m}{E_0} - pA\right)\right]}, \tag{19a}$$

where m is the contrast factor of the interference pattern, p is the exponent of the power law used for the field dependence of the charge carrier photogeneration efficiency [Eq. (5b)], and

$$A = \frac{\rho^* T_i (S_i - T_i - \rho_0)}{\rho_0(\rho_0 + T_i)(S_i - T_i)}. \tag{19b}$$

The ''fields'' are defined by

$$E_D = \frac{k_B T K}{e}, \tag{19c}$$

$$E_j = \frac{e\rho_0}{\epsilon_0 \epsilon K}, \tag{19d}$$

$$E_m = \tfrac{1}{2} C \sqrt{E_0^3}, \tag{19e}$$

$$E_q = \frac{e}{\epsilon_0 \epsilon K} \frac{\rho_0 + T_i}{1 + \frac{\rho^*}{\rho_0}\frac{T_i}{S_i - T_i}}. \tag{19f}$$

For large applied fields the diffusion field E_D can be neglected. Furthermore, the field dependence of the mobility is assumed to be weak ($C = 0$), resulting in $E_m = 0$. As in the DFWM and 2BC experiments previously carried out on the PR blends studied here, a contrast factor of the interference pattern $m = 1$ is used in the following. In the limit of low excitation, i.e., when the photogeneration rate is much smaller than the initial hole trapping rate, E_j can be neglected and A is equal to 1. The following expression for the space-charge field is then obtained:

$$E_{SC} = -E_q \frac{E_0}{(1+p)E_q + iE_0}, \tag{20a}$$

with

$$E_q = \frac{e}{\epsilon_0 \epsilon K} T_i. \tag{20b}$$

Schildkraut's model was, however, developed for the external electric field E_0 parallel to the grating vector K. In DFWM and 2BC experiments on organic PR materials, the grating vector is typically tilted with respect to the external field direction by an angle φ. Thus, the field component E_0 parallel to K will be smaller than the total applied external field $E_{0,T}$ according to

$$E_0 = E_{0,T} \cos\varphi. \tag{21}$$

Using Eqs. (20) and (21) and the approximations given above, the following relations are obtained for the amplitude $|E_{SC}|$ of the space-charge field and the phase shift ϕ for small values of φ:

$$|E_{SC}| = E_0 \left(\frac{E_q^2}{(1+p\cos^2\varphi)^2 E_q^2 + E_0^2} \right)^{1/2}, \tag{22a}$$

$$\phi = \tan^{-1}\left(\frac{E_0}{(1+p\cos^2\varphi)E_q} \right). \tag{22b}$$

Note that the dependence of $|E_{SC}|$ on the external field E_0 in the limit of $E_0 \ll E_q$ is

$$|E_{SC}|_{E_0 \ll E_q} = \frac{E_0}{(1+p\cos^2\varphi)}. \tag{23}$$

Therefore, the model predicts a decrease of the first Fourier component of the space-charge field if the charge carrier photogeneration efficiency η is strongly field dependent, which is reflected in the factor p. Furthermore, the expression of the phase ϕ contains a modified saturation field in comparison to the standard model:[11,39]

$$E_{q,\mathrm{eff}} = (1+p\cos^2\varphi)E_q. \tag{24}$$

We estimated $E_{q,\mathrm{eff}}$ based on the results of our photoelectrical experiments for parameters typically used in PR experiments: grating vector tilt angle $\varphi = 60°$ (corresponding to an average internal tilt angle of the PR grating of 30° with respect to the surface normal), $\Lambda = 3\,\mu$m, and $E_{0,T} = 60\,\mathrm{V}/\mu\mathrm{m}$, which gives $E_0 = 30\,\mathrm{V}/\mu\mathrm{m}$. As discussed above, the trap density was set to $5\times10^{16}\,\mathrm{cm}^{-3}$ and $\epsilon = 6.5$. Furthermore, $p = 2.2$ was estimated from the field dependence of the charge carrier photogeneration efficiency (Fig. 5) for a field of 60 V/μm. Calculation with Eqs. (20b), (22), and (24) yields $E_q = 69\,\mathrm{V}/\mu\mathrm{m}$, $E_{SC} = 18\,\mathrm{V}/\mu\mathrm{m}$, $E_{q,\mathrm{eff}} = 106\,\mathrm{V}/\mu\mathrm{m}$, and $\phi = 16°$. The calculated phase shift of the PR grating is in good agreement with measured values.[40] The estimate for $E_{q,\mathrm{eff}}$ should be compared to the saturation field, which is experimentally determined by comparing the diffraction efficiency and the two-beam coupling gain at the conditions given above. For PR materials with 50 wt. % DMNPAA, values of approximately 160 V/μm[15] are obtained, which is in reasonable agreement with our estimate.

Finally, we would like to correlate the previously observed change in PR performance[15] as a function of T_r to the characteristics of the photoelectrical properties as analyzed in this investigation. According to Eqs. (13) and (16) the temperature-dependent trap density will govern the T dependence of the photocurrent, as the generation rate was found to be T independent. For $T_r = 0$, T_i was set to $5\times10^{16}\,\mathrm{cm}^{-3}$ as above. The dependence of T_i on the reduced temperature is then derived from the slopes in Fig. 4(b). Knowing the field coefficient p and the illumination geometry, the first-order Fourier component of the space-charge field can be calculated according to Eq. (22a).

Since the experimental determination of the absolute value for the space-charge field is difficult, we have reanalyzed results from degenerate four wave mixing (DFWM) and electro-optical ellipsometry (ELP) on the same class of materials.[15] In these experiments the electric field E_{DFWM} necessary to reach a certain refractive index modulation Δn_{DFWM} in the DFWM experiment and the field E_{ELP} necessary to achieve a certain change Δn_{ELP} of the refractive index in the EO ellipsometry was measured for different chromophore and plasticizer concentrations. In the approximation that there is no persistent poling the following relations hold:[13,41,42]

$$\Delta n_{DFWM} = C_{DFWM}\chi_{DFWM}E_{DFWM}E_{SC}, \tag{25a}$$

$$\Delta n_{ELP} = C_{ELP}\chi_{ELP}E_{ELP}^2. \tag{25b}$$

Here, C_{DFWM} and C_{ELP} are geometrical factors, χ_{DFWM} and χ_{ELP} are effective Kerr susceptibilities, and E_{SC} is the space-charge field in the DFWM experiment at the externally applied field E_{DFWM}. Note, that for the sake of simplicity χ_{DFWM} is considered as a total effective Kerr-susceptibility, including a term for the field-induced chromophore reorientation as well as a term for the Pockels-contribution to the index modulation. Both contribute to the spatial index modulation with the same grating period as the illumination grating and, moreover, show the same field dependency as long as the bias field E_{DFWM} is constant in time or, at least, does not contain frequencies, to which the chromophores cannot respond. The projection coefficients can be assumed to be almost independent of the material composition. For χ_{DFWM} and χ_{ELP} a similar dependence on the chromophore content is expected. Consequently, the ratio

$$\frac{\Delta n_{DFWM}C_{ELP}\chi_{ELP}}{\Delta n_{ELP}C_{DFWM}\chi_{DFWM}} = \frac{E_{DFWM}E_{SC}}{E_{ELP}^2} \tag{26}$$

is the same for all experiments in Ref. 15. Thus, the magnitude of the space-charge field multiplied by a constant but unknown factor C' can be calculated:

$$\frac{E_{SC}}{E_{DFWM}} = C'\frac{E_{ELP}^2}{E_{DFWM}^2}. \tag{27}$$

E_{ELP}^2/E_{DFWM}^2 taken from Ref. 15 is plotted as a function of the reduced temperature for blends with 30, 40, and 50 wt. % chromophore content in Fig. 10. All three series show a similar dependence of the space-charge field on T_r. For $T_g < T$ the ratio E_{ELP}^2/E_{DFWM}^2 is almost constant followed by a dramatic decrease below $T_r \cong -5\,°\mathrm{C}$.

This behavior can be fully explained by the calculated temperature dependence of E_{SC}/E_0 (Fig. 10) which is based on a temperature-dependent trap density as described above. The latter calculations [Eq. (22a)] were performed for $E_{0,T} = E_{DFWM}$, $\varphi = 60°$, and $p = 2.2$. The good agreement allows to draw the following conclusions: For materials with $T_g > T$ the saturation field is almost constant and exceeds the projection of the external field on the grating wave vector (e.g., for $T_r = 19\,°\mathrm{C}$, $E_q = 109\,\mathrm{V}/\mu\mathrm{m}$, and $E_0 = 46\,\mathrm{V}/\mu\mathrm{m}$). In the limit of Eq. (23) the ratio E_{SC}/E_0 has a value of 0.64, as predicted for the PR data if $T_r > 0\,°\mathrm{C}$ (Fig. 11). For PR blends with $T_r < -5\,°\mathrm{C}$, E_q decreases significantly and E_0 becomes larger than E_q (e.g., for $T_r = -17\,°\mathrm{C}$, $E_q = 24\,\mathrm{V}/\mu\mathrm{m}$, and $E_0 = 31\,\mathrm{V}/\mu\mathrm{m}$). It is finally concluded that the dependence of the space-charge field on the reduced temperature is basically controlled by the decreased trap density in PR materials with $T_g < T$, independent of the materials composition or the absolute temperature. This finding might

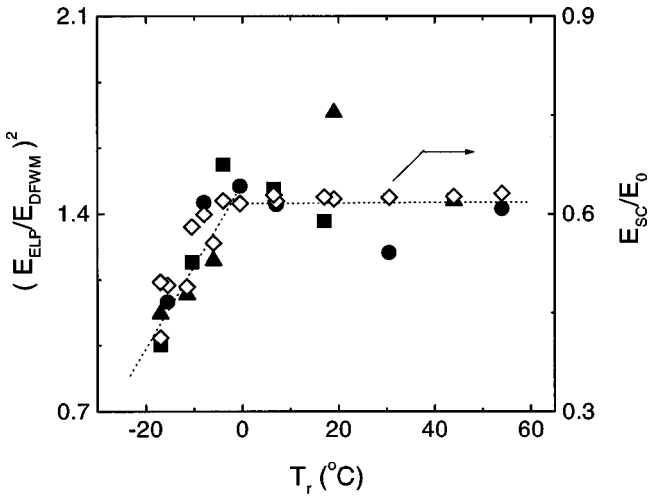

FIG. 10. Dependence of the normalized space-charge field on the reduced temperature T_r. The solid symbols (left axis) refer $(E_{\mathrm{ELP}}/E_{\mathrm{DFWM}})^2$ as defined in Eq. (27) and were calculated from the experimental data obtained from the analysis of DFWM and EO-ellipsometry experiments on PR blends with different T_g's and with 30 wt. % (triangles), 40 wt. % (circles), and 50 wt. % (squares) chromophore content (Ref. 15). The predicted theoretical dependence of the normalized space-charge field $E_{\mathrm{SC}}/E_{\mathrm{O}}$ (right axis, open diamonds) on the reduced temperature T_r was calculated according to Eq. (27) by setting $E_{O,T}=E_{\mathrm{DFWM}}$ and substituting Eqs. (22a) and (20b), respectively. The functional dependence of T_i on T_r was obtained from Fig. 4(b). The other parameters were $p=2.2$, $\varphi=60°$, and $T_i(T_r=0)=5\times10^{16}\,\mathrm{cm}^{-3}$. The dotted line serves as a guide to the eye.

also allow to identify the traps that are relevant for the space-charge field formation with conformational traps, related to hole transport in PVK. This interpretation is supported by the energy-level scheme of the components in the PR blends (Fig. 11). The ionization energy of the chromophore is found to be approximately 0.5 eV larger than that of PVK. Consequently, hole transport should primarily occur via the photoconductive moieties and not via the chromophore. In this picture, the decrease of T_i for $T_g<T$ can be explained by

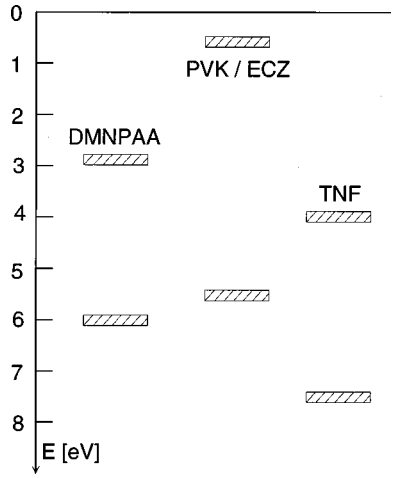

FIG. 11. Schematic energy band diagram of the components in the PVK-based PR blends. Energy levels were determined by cyclic voltammetry in acetonitrile solution and by the optical band gap of the materials.

enhanced detrapping of carriers due to faster conformational dynamics in the glass-forming material. Indeed, the shape of the master curve in Fig. 4(b) resembles the transition between the equilibrium dynamics for $T>T_g$ and the dynamics in the nonequilibrium glassy state ($T<T_g$) as typically observed in glass-forming materials.[43,44] Those conformation traps, however, possess a broad distribution of trap depths, which is often assumed to be Gaussian.[45,46] For disordered molecular solids, a width larger than 0.1 eV has been found experimentally.[46] It is expected that only ''deep'' traps in the tail of the distribution will capture charge carriers for longer times. If one assumes that each PVK repeat unit can potentially act as a trap (with $\rho_{\mathrm{PVK}}=50$ wt. % and a mass density of the solid material of 1 g/cm^3, the density of PVK repeat units is $1.5\times10^{21}\,\mathrm{cm}^{-3}$), a density of relevant traps of $5\times10^{16}\,\mathrm{cm}^{-3}$ at $T_r=0$ corresponds to a fraction of 3×10^{-5}. With a Gaussian width of 0.1 eV, only traps with a depth larger than 0.4 eV would then be relevant in the photophysical and PR experiments presented here.

We like to note that all conclusions drawn here are on the steady-state performance in the PC or PR experiment. No predictions are made for the transient PR response, which is far more complicated. For example, Grasruck *et al.*[47] have shown recently that the energy distribution of trapping sites strongly influences the grating formation speed. A detailed description of the transient behavior would require knowledge about the trapping and detrapping rates, which is not accessible by the experiments presented here.

CONCLUSION

Measurements of the field dependence of j_{dark} in materials with different glass-transition temperatures and chromophore contents as a function of temperature show a thermally activated behavior, which is, however, not related to T_g. A high activation energy $E_A=1.5$ eV is obtained. Thermal activation is also observed for the photocurrent. In contrast to the dark current, j_{photo} is related to T_g, but is independent of ρ_{CHR}. Analysis of the data with respect to the measurement temperature relative to T_g reveals a universal dependence of j_{photo} on T_r for all blends.

The charge carrier photogeneration efficiency η of the PR blends was found to be almost independent of T_g and ρ_{CHR}. Thus, a dependence of η on T_g can be excluded as a possible contribution to the universal T_r dependence of j_{photo}. The ρ_{CHR} independence indicates that the chromophore does not act as a hole acceptor in the photogeneration step, i.e., only the PVK/TNF charge-transfer complex is involved in this process. The charge carrier photogeneration efficiency of the CT complex is found to be only weakly dependent on the excitation wavelength.

Schildkraut's model was used to compare the external photocurrent efficiencies measured by photoconductivity to the photogeneration efficiencies as predicted by the Onsager fits of the η-E curves. Trap densities in the materials were determined by adjusting the photoconductivity gain factor G, which relates photocurrent efficiencies to η. Values of $T_i\approx10^{17}\,\mathrm{cm}^{-3}$ were obtained for the different materials. The similarity of the results for blends with different chromophore content suggests that the field and temperature dependence of the trap density is universal. This indicates that

the changes of the transport and recombination properties with T_g observed in photoconductivity experiments are most likely due to changes in T_i. Over the entire field range G was found to be much smaller than unity even for thin samples. The mean free path of the photogenerated charge carriers is, thus less than 1 μm, which indicates a significant recombination of the photogenerated charge carriers before they can diffuse over the distance of one grating period in typical PR experiments. According to Schildkraut's model the charged recombination centers involved in this process are not initially present in the material, but must be generated by the photoexcitation of the sensitizer.

The experimentally determined T_i was used to estimate the strength of the space-charge field in the PR material under illumination. Schildkraut's model was modified to account for the tilt between the index grating and the applied field. The universal dependence of the photocurrent on the reduced temperature was used to calculate the temperature dependence of the space-charge field in the framework of this model. The behavior predicted by our photoelectrical measurements is in excellent agreement with the relative dependence of E_{SC} on T_r obtained from the analysis of DFWM and EO-ellipsometry experiments.[15] The decrease of E_{SC} in blends with $T_g < T$ is the direct consequence of a decreased density of active traps in these materials. Since the experimental findings are satisfactorily explained by only considering thermally induced changes of the trap density, the traps involved in space-charge field formation can be identified with conformational traps.

We would like to emphasize that the experiments on the photoconductivity, the charge carrier photogeneration and the PR performance of PVK-based materials are consistently described in the framework of Schildkraut's model. While η is not affected by the trap density in the material, the decrease of T_i in materials with $T_g < T$ changes the transport and recombination properties, leading to the universal T_r dependence of j_{photo}. Furthermore, the decrease in the trap density as T_g is lowered below T decreases the maximum strength of the space-charge field. This counteracts the effect of the enhanced poling properties of the chromophore in these materials and might in part account for the optimum in PR performance of PVK-based blends with $T_g \approx T$.

ACKNOWLEDGMENTS

We would like to thank E. Mecher for measuring the absorption spectra and the phase shift of the (PR) grating, and Dr. C. Honeker for the careful reading of the manuscript. We would also like to thank Professor G. Wegner, MPI-P Mainz, and Professor C. Bräuchle, LMU Munich, for fruitful discussions. Finally, financial support by the Volkswagen Foundation, by the Bavarian government (FORMAT program) and by the Grant Agency of the Czech Republic (Grant No. 102/98/0696) is acknowledged.

*Author to whom all correspondence should be addressed.

[1] J. C. Scott, L. T. Pautmeier, and W. E. Moerner, J. Opt. Soc. Am. B **19**, 2059 (1992).
[2] B. E. Jones, S. Ducharme, M. Liphardt, and A. Goonesekera, J. Opt. Soc. Am. B **11**, 1064 (1994).
[3] G. Bäuml, S. Schloter, U. Hofmann, and D. Haarer, Opt. Commun. **154**, 75 (1998).
[4] Sandalphon, B. Kippelen, K. Meerholz, and N. Peyghambarian, Appl. Opt. **35**, 2346 (1996).
[5] A. Grunnet-Jepsen, C. L. Thompson, and W. E. Moerner, Opt. Lett. **22**, 874 (1997).
[6] A. Grunnet-Jepsen, C. L. Thompson, and W. E. Moerner, J. Opt. Soc. Am. B **15**, 905 (1998).
[7] S. Schloter, U. Hofmann, P. Strohriegl, H.-W. Schmidt, and D. Haarer, J. Opt. Soc. Am. B **15**, 2473 (1998).
[8] A. Grunnet-Jepsen, D. Wright, B. Smith, M. S. Bratcher, M. S. DeClue, J. S. Siegel, and W. E. Moerner, Chem. Phys. Lett. **291**, 553 (1998).
[9] K. S. West, D. P. West, M. D. Rahn, J. D. Shakos, F. A. Wade, K. Khand, and T. A. King, J. Appl. Phys. **84**, 5893 (1998).
[10] G. Bäuml, S. Schloter, U. Hofmann, and D. Haarer, Synth. Met. **97**, 165 (1998).
[11] N. V. Kukhtarev, V. B. Markov, S. G. Odulov, M. S. Soskin, and V. L. Vinetskii, Ferroelectrics **22**, 949 (1979).
[12] N. V. Kukhtarev, in *Photorefractive Materials and Their Applications 1*, edited by P. Günter and J.-P. Huignard (Springer, Berlin, 1988), p. 99.
[13] W. E. Moerner, S. M. Silence, F. Hache, and G. C. Bjorklund, J. Opt. Soc. Am. B **11**, 320 (1994).
[14] H. J. Bolink, V. V. Krasnikov, G. G. Malliaras, and G. Hadziioannou, J. Phys. Chem. **100**, 16356 (1996).
[15] R. Bittner, T. K. Däubler, D. Neher, and K. Meerholz, Adv. Mater. **11**, 123 (1999).
[16] I. Chen, J. Mort, and J. H. Tabak, IEEE Trans. Electron Devices **19**, 413 (1972).
[17] V. Cimrová, S. Nespurek, R. Kuzel, and W. Schnabel, Synth. Met. **7**, 103 (1994).
[18] R. H. Bube, *Photoconductivity of Solids* (Wiley, New York, 1960).
[19] T. K. Däubler, H. Rost, H.-H. Hörhold, and D. Neher, Phys. Rev. B **59**, 1964 (1999).
[20] T. K. Däubler, V. Cimrová, S. Pfeiffer, H.-H. Hörhold, and D. Neher, Adv. Mater. **11**, 1274 (1999).
[21] J. S. Schildkraut and A. V. Buettner, J. Appl. Phys. **72**, 1888 (1992).
[22] J. S. Schildkraut and Y. Cui, J. Appl. Phys. **72**, 5055 (1992).
[23] R. Bittner, C. Bräuchle, and K. Meerholz, Appl. Opt. **37**, 2843 (1998).
[24] P. Gattinger, H. Rengel, and D. Neher, Synth. Met. **83**, 245 (1996).
[25] I. D. Parker, J. Appl. Phys. **75**, 1656 (1994).
[26] P. W. M. Blom, M. J. M. de Jong, and M. G. van Munster, Phys. Rev. B **55**, R656 (1997).
[27] P. W. M. Blom, H. F. M. Schoo, and M. Matters, Appl. Phys. Lett. **73**, 3914 (1998).
[28] M. A. Lampert and P. Mark, *Current Injection in Solids* (Academic, New York, 1970).
[29] W. D. Gill, J. Chem. Phys. **57**, 1694 (1972).
[30] G. G. Malliaras, V. V. Krasnikov, H. J. Bolink, and G. Hadziioannou, Phys. Rev. B **52**, R14 324 (1995).
[31] B. Andre, R. Lever, and J. Y. Moisan, Chem. Phys. **137**, 281 (1989).

[32] P. Melz, J. Chem. Phys. **57**, 1694 (1972).
[33] T. K. Däubler, Ph.D. thesis, University of Potsdam, 1999.
[34] L. Pautmeier, R. Richert, and H. Bässler, Synth. Met. **37**, 271 (1990).
[35] C. L. Braun, J. Chem. Phys. **80**, 4157 (1984).
[36] M. Pope and C. E. Swenberg, *Electronic Processes in Organic Crystals* (Clarendon, Oxford, 1982).
[37] S. M. Silence, G. C. Bjorklund, and W. E. Moerner, Opt. Lett. **19**, 1822 (1994).
[38] J. Wolff, S. Schloter, U. Hofmann, D. Haarer, and S. J. Zilker, J. Opt. Soc. Am. B **16**, 1080 (1999).
[39] A. Grunnet-Jepsen, C. L. Thompson, R. J. Twieg, and W. E. Moerner, Appl. Phys. Lett. **70**, 1515 (1997).
[40] E. Mecher and K. Meerholz (unpublished).
[41] R. Wortmann, C. Poga, R. J. Twieg, C. Geletneky, C. R. Moylan, P. M. Lundquist, R. G. DeVoe, P. M. Cotts, H. Horn, J. E. Rice, and D. M. Burland, J. Chem. Phys. **105**, 10 637 (1996).
[42] W. E. Moerner, A. Grunnet-Jepsen, and C. L. Thompson, Annu. Rev. Mater. Sci. **27**, 585 (1997).
[43] E. Rössler and H. Sillescu, in *Material Science and Technology*, edited by R. W. Cahn, P. Haasen, and E. J. Kramer (VCH, Weinheim, 1991), Vol. 9, p. 573.
[44] H.-J. Winkelhahn, T. K. Servay, and D. Neher, Ber. Bunsenges. Phys. Chem. **100**, 123 (1996).
[45] H. Bässler, Phys. Status Solidi B **175**, 15 (1993).
[46] P. M. Borsenberger, L. Pautmeier, and H. Bässler, J. Chem. Phys. **95**, 1258 (1991).
[47] M. Grasruck, A. Schreiber, U. Hofmann, S. J. Zilker, A. Leopold, S. Schloter, C. Hohle, P. Strohriegl, and D. Haarer, Phys. Rev. B **60**, 16 543 (1999).